Journal of the Taiwan Institute of Chemical Engineers 188 (2026) 106802

Contents lists available at ScienceDirect

Journal of the Taiwan Institute of Chemical Engineers

journal homepage: www.journals.elsevier.com/journal-of-the-taiwan-institute-of-chemical-engineers

Multiscale organic–inorganic hybrid polyimides from poly(dimethyl siloxane) and double-decker silsesquioxane for balancing flexibility and thermal durability

Hui-Wen Chen, Shiao-Wei Kuo *

Department of Materials and Optoelectronic Science, Center for Functional Polymers and Supramolecular Materials, National Sun Yat-Sen University, Kaohsiung 804, Taiwan

ARTICLE INFO

Keywords:
Polyimide
Poly(dimethyl siloxane)
Double-decker silsesquioxane (DDSQ)
Surface property
Dielectric Property

ABSTRACT

Background: Hybrid silicone–aromatic polyimides that combine high thermal stability, surface hydrophobicity, and low dielectric constants are highly desirable for advanced microelectronic and insulating applications. However, simultaneously integrating flexibility, thermal robustness, and dielectric performance within the single polyimide system remains challenging because of their intrinsic trade-offs between rigid aromatic backbones and flexible siloxane segments. As a result, incorporating inorganic double-decker silsesquioxane (DDSQ) cage structure could offer the promising strategy to overcome these limitations by reinforcing polymer matrices while preserving processability and functional tunability.

Methods: Hybrid polyimides containing flexible poly(dimethyl siloxane) (PDMS) segments and rigid double-decker silsesquioxane (DDSQ) nanocages were synthesized via a nadic anhydride-mediated molecular design. Hydride-terminated PDMS and DDSQ were first functionalized with nadic anhydride through Pt-catalyzed hydrosilylation to afford telechelic anhydride-terminated precursors, followed by ring-opening reactions with aromatic diamines (ODA and PPD) to form diamine-functionalized silicone intermediates. Subsequent polycondensation with pyromellitic dianhydride (PMDA) produced silicone-containing poly(amic acid)s, which were converted into polyimide films through stepwise thermal imidization. Structural and morphological characteristics were analyzed by FTIR, SEM, TEM, and elemental mapping.

Significant findings: The resulting PDMS/DDSQ hybrid polyimides with a fixed PDMS/DDSQ weight ratio of 80/20 exhibited homogeneous organic–inorganic architectures with uniform nanoscale dispersion of DDSQ cages within the polyimide matrix. DDSQ incorporation significantly enhanced thermal stability and char yield while preserving the film flexibility imparted by PDMS. Surface analyses revealed increased hydrophobicity and markedly reduced surface free energy due to preferential silicone enrichment at the film surface. Dielectric measurements further demonstrated that the synergistic combination of low-polarizable PDMS chains and rigid DDSQ nanocages effectively suppressed dielectric polarization, leading to reduced dielectric constants, particularly in the hybrid systems. Overall, this study establishes an effective molecular design strategy for balancing thermal, surface, and dielectric properties in silicone-based polyimides for next-generation electronic and insulating applications.

1. Introduction

Polyimides (PIs) are the most important classes of high-performance polymers because of their excellent thermal stability, chemical resistance, mechanical robustness, and dielectric reliability, which make them applied in aerospace, microelectronics, and advanced insulating applications [1–5]. Nonetheless, conventional fully aromatic PIs typically suffer from poor processability, inherent brittleness, and relatively high dielectric constants arising from densely packed rigid chains and strong intermolecular interactions [6,7]. Those limitations have motivated extensive studies to modify PI backbones through molecular engineering to achieve the balance between thermal durability, flexibility, thermal durability, low surface free energy and low dielectric behavior [8–10].

* Corresponding author.
E-mail address: kuosw@faculty.nsysu.edu.tw (S.-W. Kuo).

https://doi.org/10.1016/j.jtice.2026.106802
Received 22 January 2026; Received in revised form 22 April 2026; Accepted 28 April 2026
Available online 5 May 2026

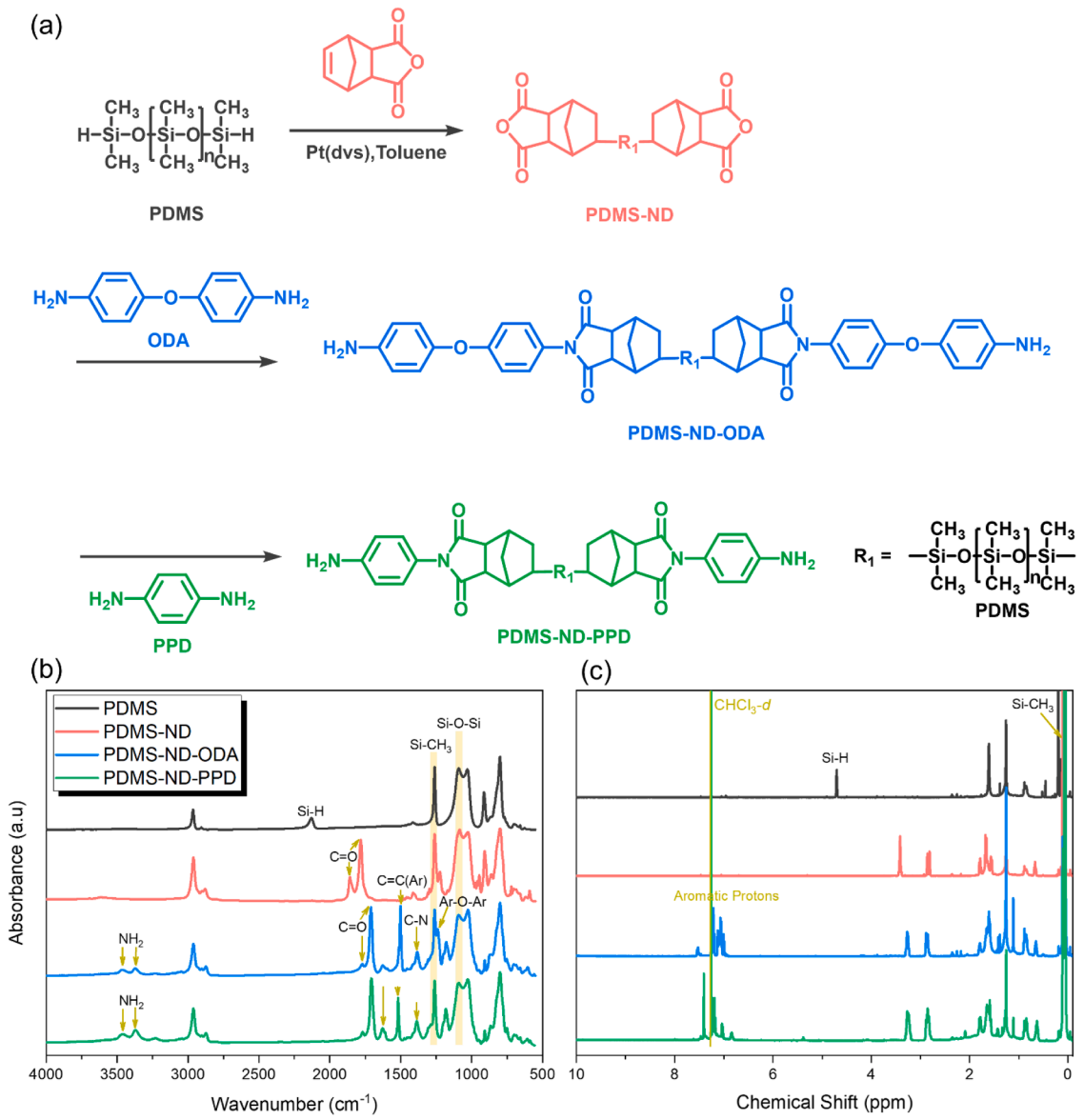

Fig. 1. (a) Syntheses of PDMS-ND, PDMS-ND-ODA and PDMS-ND-PPD diamine intermediates and their corresponding (b) FTIR and (c) ^{1}H NMR.

Incorporation of silicone segments into PIs has emerged as an effective strategy to improve chain flexibility and reduce the dielectric constants due to the low polarity and high free volume associated with Si-O-Si linkages [11–15]. PDMS-containing PIs exhibit improved toughness, flexibility, surface hydrophobicity, and lower *k* values; nevertheless, the introduction of flexible siloxane chains often leads to reduce the thermal stability and mechanical strength [16–18]. Therefore, the integration of rigid inorganic nanostructures capable of reinforcing into the polymer matrix while retaining the beneficial properties of silicone is highly desirable.

Polyhedral oligomeric silsesquioxanes (POSS) [19–24] or double-decker silsesquioxane (DDSQ) [25–27] possess unique cage-type inorganic building blocks with well-defined nanometer dimension (1–3 nm), high thermal resistance, and strong Si–O-Si frameworks [28–30]. Embedding these nanocages into the polymer backbones has been exhibited to significantly enhance thermal stability, mechanical rigidity, and char yield while introducing intrinsic free volume beneficial for lower dielectric constant [31–33]. Among them, the difunctionalized DDSQ nanocages offer the rigid silsesquioxane architecture that could act as an effective molecular nano-reinforcement when covalently integrated into polymer main chains [34–36].

A promising route to covalently bond link flexible silicone segments and inorganic cages into PI architectures involves hydrosilylation of nadic anhydride (ND) onto Si–H-terminated species, followed by diamine ring opening and subsequent PI formation [37,38]. This approach allows precise end-functionalization and introduces reactive anhydride groups without disrupting the silicone backbone. Despite several reports on PDMS-PI or POSS-PI organic/inorganic hybrids, systematic construction of PDMS/DDSQ hybrid polyimides or other polymers via nadic chemistry and their multiscale structural characterizations remain largely unexplored. The novelty of this study lies in the simultaneous incorporation of flexible PDMS segments and rigid DDSQ nanocages into a single polyimide system, which has been rarely explored and this dual-component design enables a unique balance between chain mobility and structural rigidity.

In this study, we propose a modular synthetic strategy to construct hybrid silicone–aromatic PIs by combining flexible PDMS chains and rigid DDSQ nanocages through ND-mediated functionalization, diamine coupling (4,4′-oxydianiline (ODA), *p*-phenylenediamine (PPD)), and subsequent polymerization with pyromellitic dianhydride (PMDA). The resulting PDMS-PI, DDSQ-PI, and hybrid PDMS/DDSQ-PI films were comprehensively characterized by FTIR, NMR, SEM, TEM, and

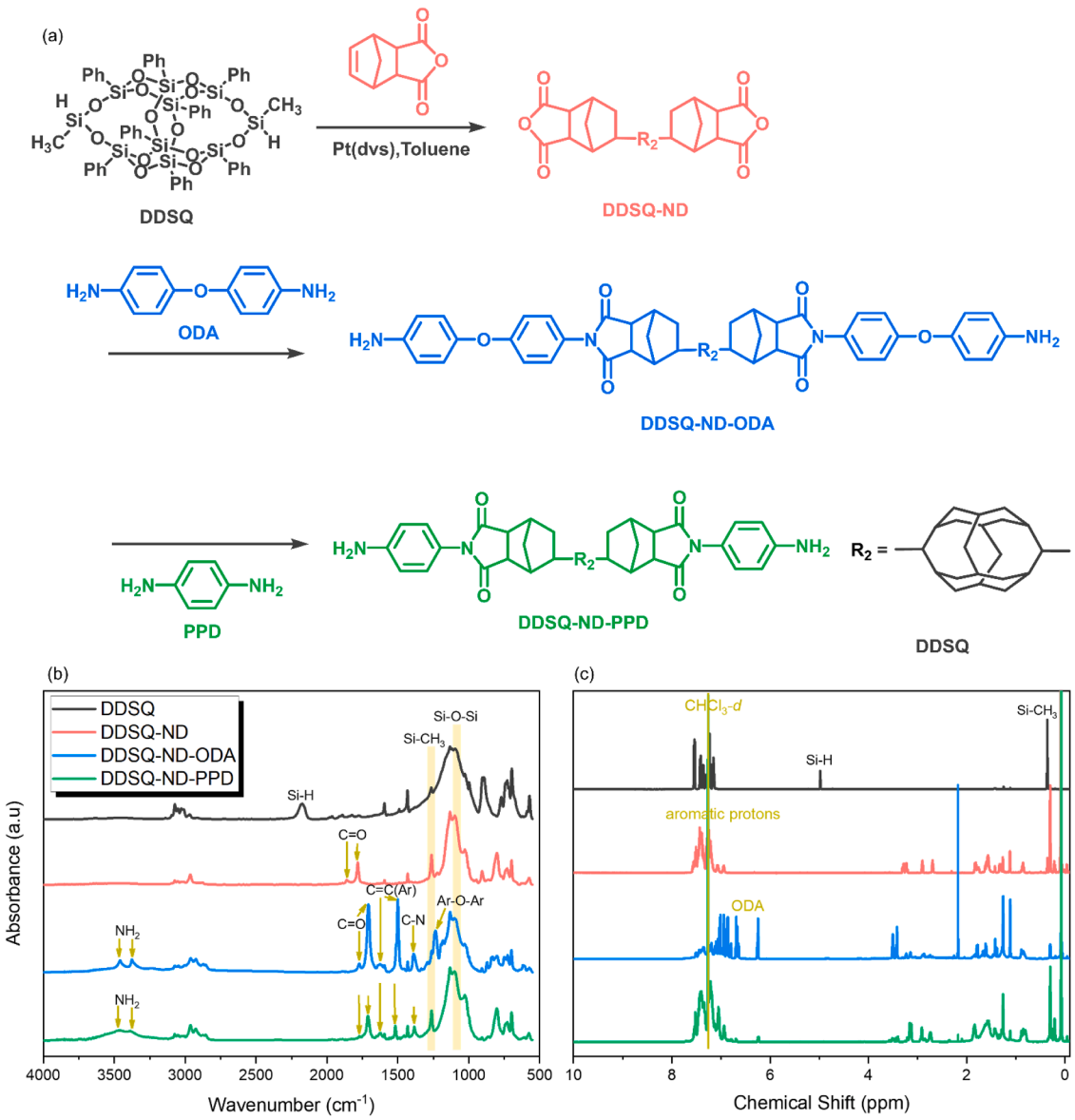

Fig. 2. (a) Syntheses of DDSQ-ND, DDSQ-ND-ODA and DDSQ-ND-PPD diamine intermediates and their corresponding (b) FTIR and (c) ^{1}H NMR.

elemental mapping to elucidate their molecular and nanoscale structures. Furthermore, their thermal stability, hydrophobicity, surface free energy, and dielectric properties were systematically investigated by TGA and contact angle analyses. This study demonstrates that synergistic integration of soft siloxane segments and rigid DDSQ nanocages provides a powerful route to tune polyimide performance for next-generation low-*k* and thermally robust materials.

2. Experimental section

2.1. Materials

5-Norbornene-2,3-dicarboxylic anhydride (nadic anhydride) and hydride-terminated poly(dimethylsiloxane) (PDMS, M_n = 580 g mol^{-1}) were purchased from Sigma-Aldrich. Toluene, tetrahydrofuran (THF) and N,N-dimethylacetamide (DMAc) were purchased from Merck and were dried over CaH_2 for 24 h. Platinum(0)-1,3-divinyl-1,1,3,3-tetramethyldisiloxane [Pt(dvs)], 4,4′-oxydianiline (ODA), *p*-phenylenediamine (PPD) an were purchased from Alfa-Aesar. Bis(nadic anhydride)-terminated d pyromellitic dianhydride (PMDA) poly (dimethyl siloxane) (PDMS-ND) was synthesized according to our previously reported procedure (Fig. 1a) [39]. Double-decker silsesquioxane (DDSQ) and bis(nadic anhydride)-functionalized DDSQ (DDSQ-ND) were prepared following methods described in our earlier studies (Fig. 2a) [40–43].

2.2. Syntheses of PDMS-ND-ODA and PDMS-ND-PPD

PDMS-ND (2.09 g) and 4,4′-oxydianiline (ODA, 3.00 g) or *p*-phenylenediamine (PPD, 1.49 g) were charged into a two-necked round-bottom flask equipped with a reflux condenser. Toluene (20 mL) was added, and the mixture was stirred at 105 °C for 48 h. After completion of the reaction, the solvent was removed using a rotary evaporator, and the residue was further dried in a vacuum oven at 130 °C to afford a brown solid of PDMS-ND-ODA (yield: 92 %) and a dark-brown solid of PDMS-ND-PPD (yield: 84 %) (Fig. 1a).

2.3. Synthesis of DDSQ-ND-ODA and DDSQ-ND-PPD

DDSQ-ND (11.80 g) with 4,4′-oxydianiline (ODA) (9.60 g) or p-phenylenediamine (PPD) (4.80 g) were placed into the two-necked round-bottomed flask with the reflux condenser, dropwise toluene

(240 mL) and stir for a while. It was then heated to 105 °C for 2 days under N_2 atmosphere. The solution was removed by rotary distillation under vacuum and then placed in vacuum oven at 180 °C for 3 days to provide a brownish yellow solid for DDSQ-ND-ODA (yield: 87 %) and black solid product for DDSQ-ND-PPD (yield: 82 %) as shown in Fig. 2 (a).

2.4. Syntheses of PDMS-ODA PI and PDMS-PPD polyimide (PI) films

PDMS-ND-ODA (1.0 g) or PDMS-ND-PPD (1.0 g) was dissolved in a mixed solvent of DMAc/THF (10 mL, 1/1 v/v) in a 25 mL three-neck flask equipped with a mechanical stirrer. Pyromellitic dianhydride (PMDA, 0.17 g for PDMS-ND-ODA or 0.20 g for PDMS-ND-PPD) was added portionwise under stirring to initiate poly(amic acid) (PAA) formation. The reaction was allowed to proceed at room temperature for 48 h to yield a homogeneous and viscous poly(amic acid) (PAA) solution. For film preparation, the pale-beige PDMS-ODA PAA or the brown PDMS-PPD PAA solution was blade-cast onto copper substrates and subjected to stepwise thermal imidization under air at 60, 80, 100, 150, 200, and 300 °C, each for 1 h, to obtain flexible PDMS-based PI film for PDMS-ODA PDI or PDMS-PPD PI.

2.5. Syntheses of DDSQ-ODA and DDSQ-PPD PI film

DDSQ-ND-ODA (1.0 g) or DDSQ-ND-PPD (1.0 g) was dissolved in DMAc in a 25 mL three-neck flask. Pyromellitic dianhydride (PMDA, 0.12 g for DDSQ-ND-ODA or 0.14 g for DDSQ-ND-PPD) was added gradually under continuous stirring. The reaction mixture was maintained at room temperature for 48 h to afford a viscous PAA solution. PI films were prepared from 20 wt % beige DDSQ-ODA PAA and brown DDSQ-PPD PAA solutions, which were cast onto glass plate followed by stepwise thermal imidization under air at 60, 80, 100, 150, 200, and 300 °C, each for 1 h, to obtain DDSQ-ODA PI and DDSQ-PPD PI films. In addition, hybrid silicone polyimides composed of PDMS and DDSQ at a PDMS/DDSQ weight ratio of 80/20 were prepared by combining the flexible PDMS-based PI with the rigid DDSQ-based PI using the same synthetic and thermal imidization procedures described above, yielding PDMS/DDSQ-ODA PI and PDMS/DDSQ-PPD PI films.

3. Results and discussion

3.1. Syntheses of PDMS-ND-ODA and PDMS-ND-PPD diamine derivatives

Hydride-terminated PDMS was first functionalized with nadic anhydride through Pt(dvs)-catalyzed hydrosilylation in toluene to introduce terminal cyclic anhydride groups (PDMS-ND), as shown in Fig. 1 (a). The hydrosilylation reaction was proceeded yielding a telechelic PDMS precursor suitable for further imide-forming reactions. Subsequent nucleophilic ring-opening reactions between PDMS-ND and aromatic diamines, including ODA and PPD, afforded the corresponding diamine PDMS-ND-ODA and PDMS-ND-PPD derivatives. Fig. 1(b) shows FTIR spectra of pure PDMS, PDMS-ND, PDMS-ND-ODA, and PDMS-ND-PPD. The Si–H stretching band at ca. 2130 cm^{-1} observed in PDMS nearly disappeared after hydrosilylation, confirming quantitative consumption of terminal Si–H groups. Concurrently, two characteristic anhydride carbonyl absorptions at 1860 and 1780 cm^{-1} emerged in PDMS-ND, indicative of successful grafting of nadic anhydride onto the PDMS chain ends. After reaction with ODA or PPD, these anhydride bands were replaced by 1770–1768 cm^{-1} and 1708 cm^{-1} were given to symmetrical and asymmetrical stretching vibrations of carbonyl groups of imide rings. In addition, the aromatic C=C stretching (1600 and 1500 cm^{-1}) and N–H stretching bands at 3463–3458 cm^{-1} and 3372–3370 cm^{-1}, corresponding to asymmetrical and symmetrical vibration, further confirmed incorporation of ODA and PPD moieties. Importantly, the Si–O–Si absorption at 1092 cm^{-1} and Si-CH_3 unit at 1261 cm^{-1} remained unchanged, demonstrating that the PDMS backbone was chemically preserved during functionalization and successful formation of the diamine adduct. The ^{1}H NMR spectra of PDMS-ND-ODA and PDMS-ND-PPD (Fig. 1(c) and Figure S1(a)) exhibit the characteristic PDMS Si–CH_3 resonance at 0.19 ppm alongside newly appeared aromatic proton signals between 6.94 and 7.50 ppm arising from the ODA units and 6.83 and 7.40 ppm arising from the PPD units. The absence of Si-H signal after the hydrosilylation with ND to produce PDMS-ND, and the aliphatic protons appeared between 0.88 and 3.41 ppm, correspond to the nadic bridge protons, further supporting successful end-functionalization and diamine attachment.

3.2. Syntheses of DDSQ-ND-ODA and DDSQ-ND-PPD diamine derivatives

To construct rigid silsesquioxane-based imide precursors, DDSQ was first end-functionalized with ND via Pt(dvs)-catalyzed hydrosilylation, yielding DDSQ-ND. The reactive anhydride termini were subsequently coupled with aromatic diamines, including ODA and PPD, to form DDSQ-ND-ODA and DDSQ-ND-PPD, respectively, as shown in Fig. 2(a). The stepwise functionalization was confirmed by FTIR and ^{1}H NMR spectroscopy, as summarized in Fig. 2(b) and (c). The FTIR spectra of pristine DDSQ exhibits characteristic Si–O–Si stretching bands centered at 1132 cm^{-1} together with Si–CH_3 vibrations near 1263 cm^{-1}. After hydrosilylation with nadic anhydride, DDSQ-ND shows the appearance of strong anhydride carbonyl absorptions at 1858 and 1780 cm^{-1}, accompanied by a reduction of the Si–H stretching signal (~2180 cm^{-1}), indicating successful addition across the norbornene double bond. Following reaction with ODA or PPD (Fig. 2b), the anhydride carbonyl bands disappear and are replaced by new imide C=O absorptions at 1773–1770 cm^{-1} and 1713–1706 cm^{-1}, confirming nucleophilic ring opening by the diamine. Additional peaks at ~1600 and 1500 cm^{-1} correspond to aromatic C=C stretching. A broad N–H stretching band at 3463–3454 cm^{-1} and 3383–3379 cm^{-1}, corresponding to asymmetrical and symmetrical vibration, further confirmed incorporation of ODA and PPD moieties, further supports successful incorporation of the diamine. The preservation of Si–O–Si skeletal vibrations demonstrates that the DDSQ cage remains intact during functionalization.

The ^{1}H NMR spectra provide additional molecular-level evidence for successful coupling as shown in Fig. 2(c) and S1(b). Firstly, the Si-H protons signal at 4.98 ppm disappeared through hydrosilylation with ND and there are some peaks between 1.2 and 3.2 ppm arise from the nadic bridge methylene and methine protons. Secondly, no residual norbornene vinyl proton signals are detected, confirming hydrosilylation. Finally, DDSQ-ND-ODA and DDSQ-ND-PPD show strong Si–CH_3 resonance near 0.30 ppm, characteristic of the silsesquioxane framework. As shown in Figure S1(b), The multiple resonances observed in the Si–CH_3 region are assigned to chemically nonequivalent Si–CH_3 groups generated after reaction of the Si–H-containing DDSQ precursor with ND (DDSQ-ND). This reaction alters the local chemical environment around the silsesquioxane cage and lowers the molecular symmetry, resulting in several Si–CH_3 resonances rather than a single peak. Therefore, the signals at 0.36, 0.30, and 0.21 ppm are attributed to Si–CH_3 groups in different substituted/isomeric DDSQ environments. The multiple resonances in the Si–CH_3 region are attributed not only to symmetry lowering of the DDSQ cage after functionalization, but also to the formation of regioisomeric products (α- and β-addition) during hydrosilylation of the Si–H groups with ND. These distinct addition modes generate chemically nonequivalent Si–CH_3 environments, resulting in multiple signals at 0.36, 0.30, and 0.21 ppm. After further modification with ODA or PPD, the local chemical environments become partially homogenized and/or the relative populations of these environments change, which leads to attenuation of certain resonances (notably the 0.30 ppm signal in DDSQ-ND-ODA) and a simplified Si–CH_3 spectral pattern. Aromatic protons from the ODA and PPD moieties appear in the 6.5–7.6 ppm region and the consistent siloxane methyl

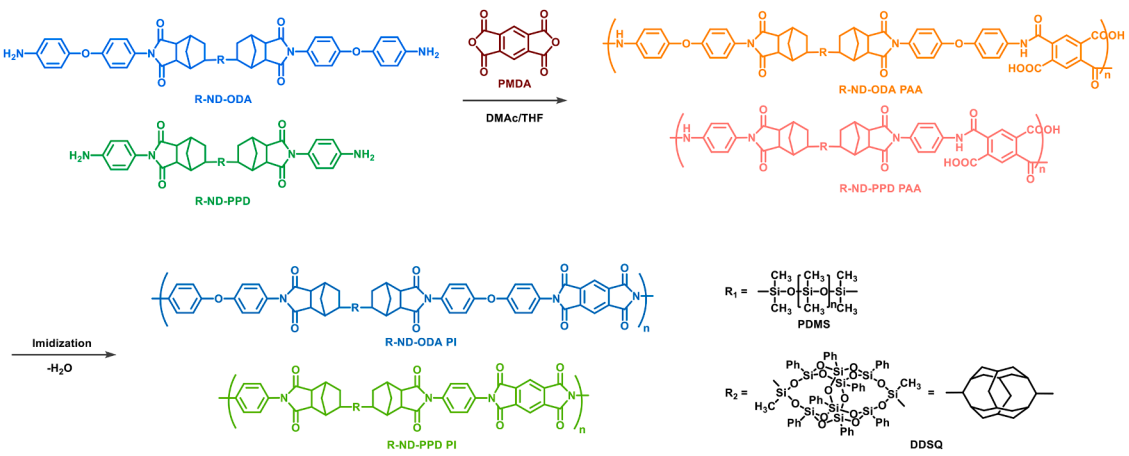

Scheme 1. The synthesis of PDMS-ND and DDSQ-ND diamine derivatives to form poly(amic acid) and polyimide.

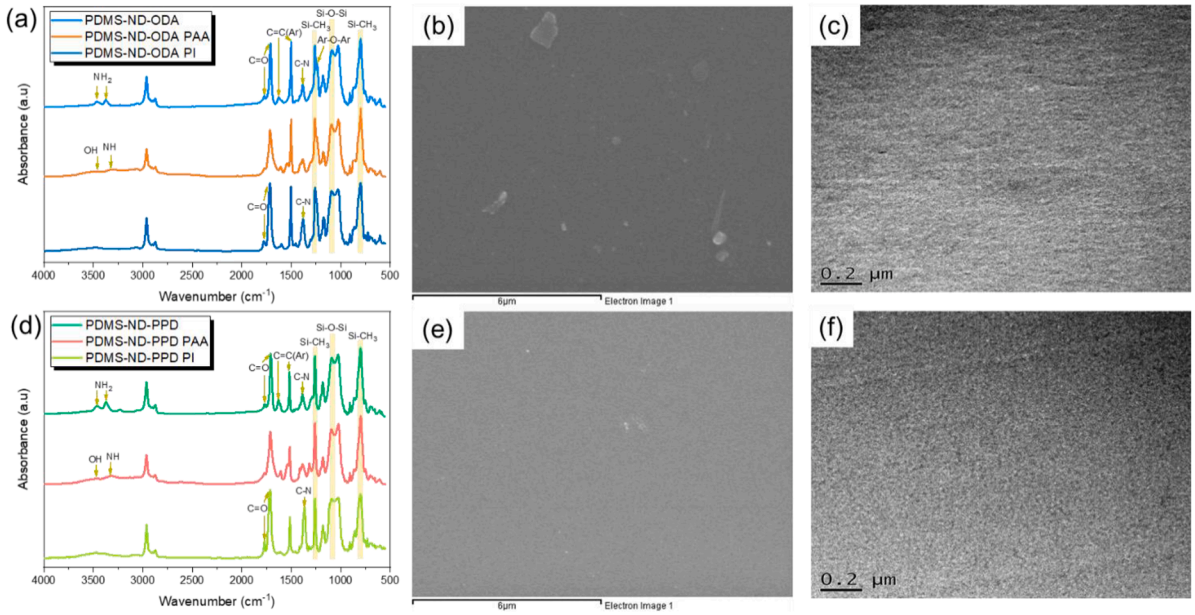

Fig. 3. (a, d) FTIR analyses, (b, e) SEM images and (c, f) TEM images of (a, b, c) PDMS-ND-ODA PI and (d, e, f) PDMS-ND-PPD PI systems.

signals and absence of unsaturated peaks further verify quantitative functionalization. These spectroscopic results (Figs. 1 and 2) confirm that nadic anhydride groups were successfully introduced onto PDMS and DDSQ through hydrosilylation and subsequently reacted with aromatic diamines to generate well-defined rigid imide precursors. The flexible PDMS or intact DDSQ cage combined with terminal aromatic segments with diamine units establishes a highly flexible PDMS or rigid DDSQ molecular architecture that is expected to enhance thermal stability and tunable mechanical robustness in the resulting silicone-based polyimide systems.

3.3. Design and synthesis of silicone-based polyimides from Nadic-functionalized PDMS and DDSQ precursors

The overall synthetic strategy for constructing the PDMS- and DDSQ-containing polyimides is illustrated in Scheme 1. The approach is based on combining flexible siloxane and rigid DDSQ molecular architecture segments with rigid aromatic imide backbones through nadic-anhydride-functionalized intermediate and the resulting ND–diamine-functionalized PDMS and DDSQ precursors were then polymerized with pyromellitic dianhydride (PMDA) in DMAc/THF to form the corresponding poly(amic acid) (PAA) intermediates. Because both chain ends carry amine functionalities after nadic ring opening, step-growth polymerization proceeds to afford high-molecular-weight silicone–aromatic hybrid PAAs. Finally, thermal imidization of the PAAs led to the formation of PDMS- and DDSQ-containing polyimides with the elimination of water. This imidization step converts the amic acid groups into imide rings, locking the rigid aromatic framework while maintaining the silicone segments within the polymer backbone.

The transformation of PDMS-ND-diamine intermediates into poly (amic acid) (PAA) precursors and subsequently into polyimide (PI) films was verified by FTIR spectroscopy and further examined by SEM and TEM to evaluate film homogeneity and nanoscale morphology (Fig. 3). For both PDMS-ND-ODA (Fig. 3a) and PDMS-ND-PPD (Fig. 3d) systems, the precursor spectra display amide and aromatic absorptions derived from nadic-opened diamine structures. After reaction with PMDA, the PAA intermediates exhibit broad carbonyl bands at 1715–1665 cm^{-1} assigned to amic acid groups. Following stepwise thermal curing, these bands disappear and are replaced by characteristic imide absorptions at 1780 and 1720 cm^{-1} along with imide ring deformation near 1380 cm^{-1}, confirming successful cyclodehydration. The invariant Si–O–Si bands (ca. 1100 cm^{-1}) indicate that the PDMS backbone remains intact

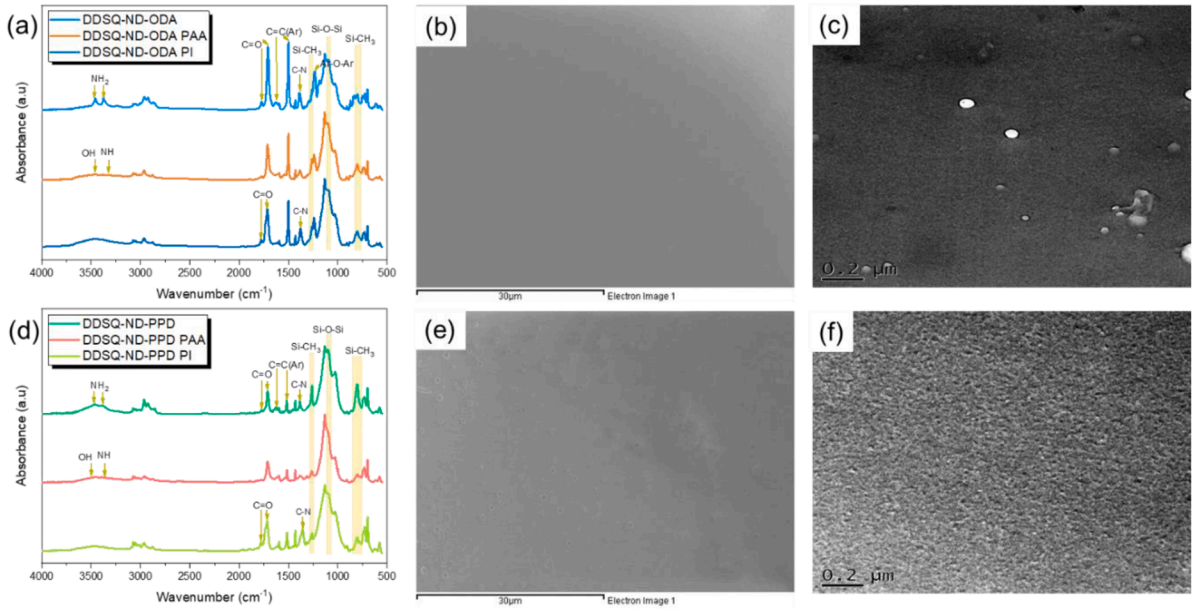

Fig. 4. (a, d) FTIR analyses, (b, e) SEM images and (c, f) TEM images of (a, b, c) DDSQ-ND-ODA PI and (d, e, f) DDSQ-ND-PPD PI systems.

throughout the polymerization and imidization processes. SEM images show continuous and defect-free surfaces for both PI films. The PDMS-ND-ODA film (Fig. 3b) exhibits a relatively smooth morphology with slight surface undulations, reflecting enhanced chain mobility from the ether-linked ODA segment. In contrast, the PDMS-ND-PPD film (Fig. 3e) displays a more uniform and compact texture, consistent with the increased rigidity of the para-phenylene unit that promotes tighter molecular packing. No phase separation or aggregation is observed at the micrometer scale, demonstrating good compatibility between the flexible siloxane segments and rigid aromatic imide domains. TEM images provide nanoscale insight into the internal structure of the cured films. Both samples reveal homogeneous contrast without distinct microdomains, suggesting that PDMS chains are well-dispersed within the aromatic polyimide matrix. The ODA-based system shows slightly lighter and more diffuse regions, attributable to localized free volume associated with flexible ether linkages as shown in Fig. 3(c). The PPD-based PI presents a denser and more uniform contrast, indicative of a higher packing density and reduced segmental mobility as shown in Fig. 3(f). The absence of obvious nanophase separation confirms that the silicone segments are covalently integrated rather than forming isolated PDMS-rich domains.

The structural conversion of DDSQ-ND-diamine precursors into poly (amic acid) intermediates and subsequently into DDSQ-containing polyimide (PI) films was confirmed by FTIR spectroscopy, while the surface and nanoscale morphologies were examined using SEM and TEM analyses (Fig. 4). For the DDSQ-ND-ODA system (Fig. 4a), the precursor shows the characteristic amide and aromatic absorptions originating from ODA groups attached to the DDSQ cage. After reaction with PMDA, new broad bands appear in the 1710–1660 cm^{-1} region, corresponding to amic acid carbonyl stretching, confirming successful formation of DDSQ-based PAA. Following thermal imidization, these bands disappear and are replaced by strong imide carbonyl absorptions at 1780 and 1720 cm^{-1} along with imide skeletal vibrations near 1380 cm^{-1}. The Si–O–Si framework bands (ca. 1130 cm^{-1}) remain unchanged throughout, demonstrating that the DDSQ cage structure is preserved during polymerization and curing. In the DDSQ-ND-PPD series (Fig. 4d), similar spectral evolution is observed. The PAA intermediate displays prominent amic acid carbonyl absorptions that are fully converted into imide bands after thermal treatment. Compared to the ODA-based system, the PPD-derived PI exhibits sharper and more intense imide peaks, reflecting higher rigidity and more ordered chain packing introduced by the para-phenylene linkage. SEM images reveal distinct differences between the ODA- and PPD-based DDSQ PI films. The DDSQ-ND-ODA PI film (Fig. 4b) presents a smooth and uniform surface without visible aggregation, indicating good compatibility between DDSQ cages and the aromatic imide matrix when flexible ether-containing ODA linkers are used. Conversely, the DDSQ-ND-PPD PI film (Fig. 4e) shows numerous circular microvoid-like features distributed across the surface. These

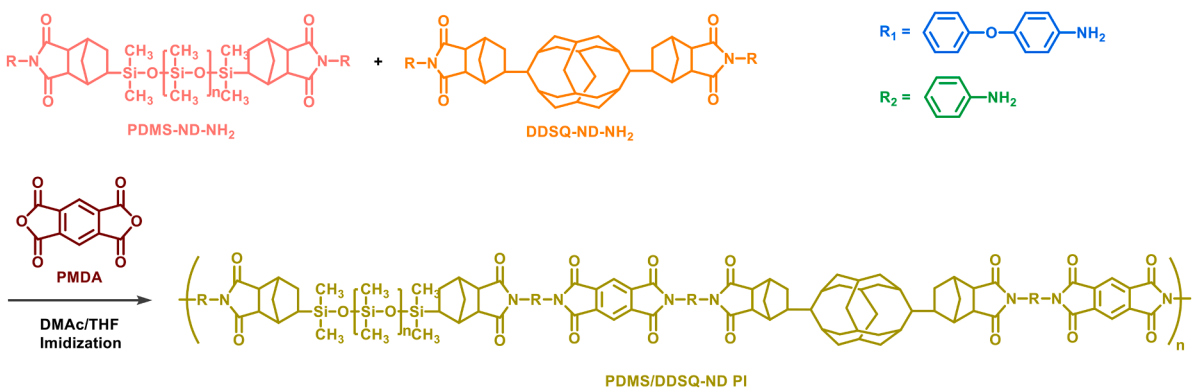

Scheme 2. The synthesis of PDMS/DDQ-ND PI system from PDMS and DDSQ-ND diamine derivatives.

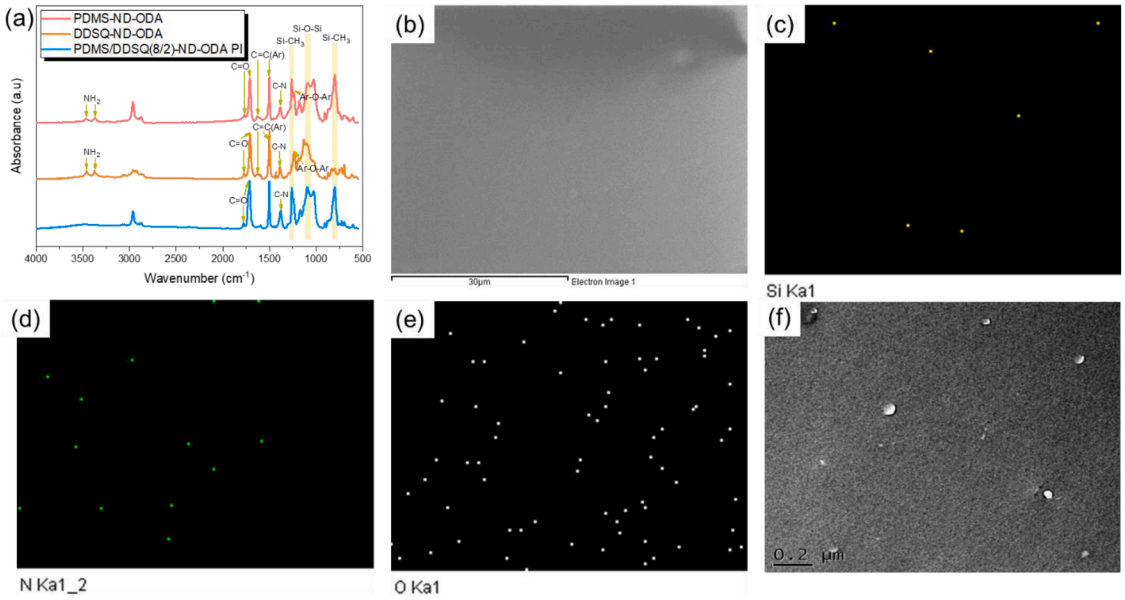

Fig. 5. (a) FTIR analyses, (b) SEM image and their corresponding EDS mapping (the same scale bar of SEM image) of (c) Si, (d) N, (e) O and (f) TEM image of PDMS/DDSQ-ND-ODA PI.

features likely arise from local packing constraints and internal stress generated by the highly rigid PPD segments combined with bulky DDSQ cages during solvent evaporation and imidization. TEM further highlights nanoscale structural differences. The DDSQ-ND-ODA PI film exhibits relatively uniform contrast with only minor dispersed darker domains, suggesting homogeneous distribution of DDSQ cages within the imide network as shown in Fig. 4(c). In contrast, the DDSQ-ND-PPD PI film displays dense and grain-like textures across the entire region as shown in Fig. 4(f), indicative of tighter packing and possible nanoscale aggregation of DDSQ-rich domains due to reduced chain flexibility. The darker contrast corresponds to the high electron density of the silsesquioxane cage cores embedded in the organic matrix.

Figs. 3 and 4 demonstrate successful synthesis of PDMS and DDSQ-based aromatic polyimides through nadic-functionalized PDMS and DDSQ precursors. FTIR confirms complete imidization, while SEM and TEM reveal that diamine rigidity strongly influences microstructure. Flexible ODA promotes uniform dispersion and smooth film morphology, whereas rigid PPD induces denser PDMS and DDSQ packing at the nano-scale.

3.4. *Molecular design and synthesis of hybrid PDMS/DDSQ-Containing polyimides*

Scheme 2 illustrates the synthetic strategy employed to construct hybrid silicone–aromatic polyimides by integrating flexible PDMS segments and rigid double-decker silsesquioxane (DDSQ) nanocages into a PMDA-based imide backbone through nadic-anhydride-mediated coupling. The incorporation ratio between PDMS and DDSQ was fixed at 80/20 (w/w), allowing simultaneous introduction of soft siloxane chains and rigid silsesquioxane cages into the polymer backbone, which produces a multiscale organic–inorganic hybrid framework. This molecular design enables the combination of high thermal stability and mechanical robustness from DDSQ and aromatic imide units with the flexibility and processability imparted by PDMS chains that demonstrates a modular copolymerization approach to precisely integrate cage-type inorganic nanostructures and soft silicone segments within a single polyimide backbone. In addition, our preliminary studies indicated that higher DDSQ loadings led to increased synthetic difficulty and reduced reproducibility, likely due to steric hindrance and the lower reactivity of DDSQ-containing intermediates, which complicated polymerization and purification. Based on these considerations, we focused on the 80/20 composition as a representative system to demonstrate the synergistic effects of PDMS and DDSQ in this study.

The chemical composition and microstructural homogeneity of the PDMS/DDSQ-ND-ODA hybrid PI film were investigated by FTIR spectroscopy, SEM, elemental mapping via energy-dispersive X-ray spectroscopy (EDS) and TEM analyses as shown in Fig. 5. The FTIR spectra (Fig. 5a) compares PDMS-ND-ODA, DDSQ-ND-ODA, and the hybrid PDMS/DDSQ-ND-ODA PI system. Both PDMS- and DDSQ-derived intermediates exhibit characteristic amide/anhydride-derived absorptions prior to polymerization. In the hybrid sample, all key vibrational bands from the silicone segments and aromatic components coexist, indicating successful incorporation of both flexible PDMS chains and rigid DDSQ cages into a single precursor structure. The preserved Si-O-Si bands confirm that the inorganic siloxane framework remains intact after reaction. In addition, the chemical structure evolution from poly(amic acid) (PAA) to polyimide (PI) was confirmed by FTIR spectroscopy, as shown in Figure S2. Enlarged views of the carbonyl (C=O) and C–N stretching regions are provided to clearly illustrate the characteristic changes. For the PAA samples, characteristic absorption bands corresponding to amic acid structures are observed, including the amide C=O stretching around ~1650 cm^{-1} and the carboxylic acid C=O stretching near ~1720 cm^{-1}. These features confirm the successful formation of the poly(amic acid) intermediates. After thermal imidization, the spectra of PI samples exhibit significant changes in the carbonyl region. The characteristic imide carbonyl absorptions appear at approximately ~1780 cm^{-1} (asymmetric C=O stretching) and ~1720 cm^{-1} (symmetric C=O stretching), accompanied by the disappearance or significant reduction of the amide-related bands. In addition, the imide C–N stretching vibration around ~1370 cm^{-1} becomes more prominent. These spectral changes clearly indicate the successful conversion from PAA to PI structures. Similar trends are observed for both PDMS- and DDSQ-containing systems, confirming that the incorporation of hybrid segments does not hinder the imidization process.

SEM imaging (Fig. 5b) reveals a continuous and uniform film surface over a 30 μm scale without visible cracks or large phase-separated domains. The smooth morphology suggests good compatibility between the PDMS soft segments and DDSQ rigid nanostructures within the polyimide matrix. Elemental mapping of the hybrid PI film provides direct evidence of homogeneous dispersion of organic and inorganic

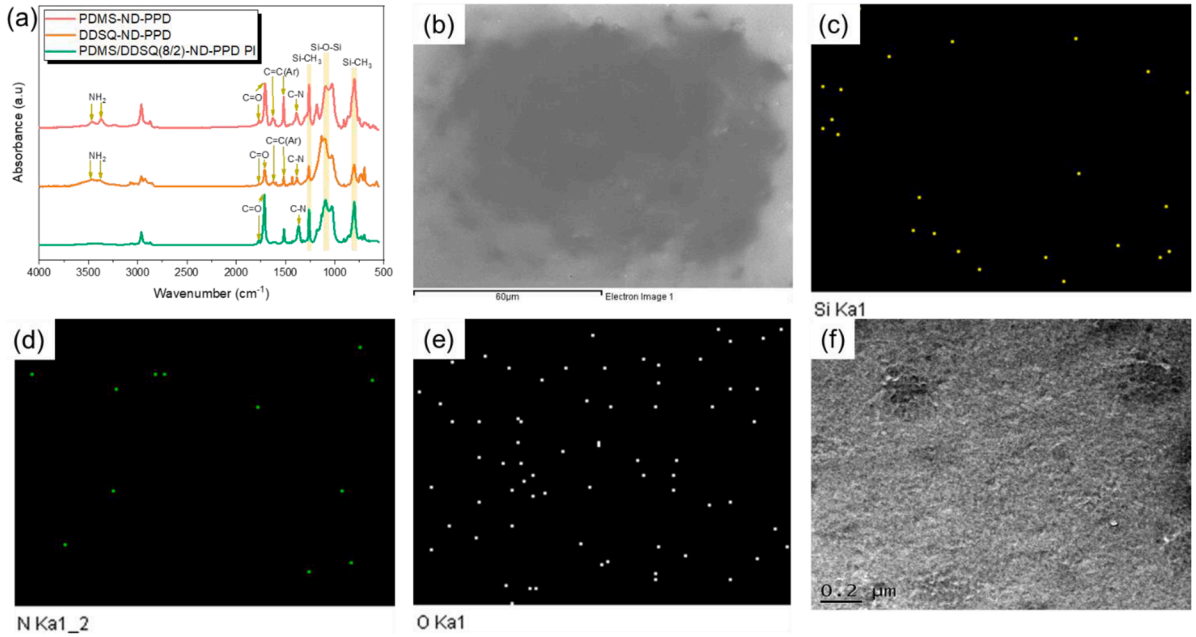

Fig. 6. (a) FTIR analyses, (b) SEM image and their corresponding EDS mapping (the same scale bar of SEM image) of (c) Si, (d) N, (e) O and (f) TEM image of PDMS/DDSQ-ND-PPD PI.

components including N (green color, Fig. 5d) from the presence of imide/amide-derived nitrogen from aromatic diamine segments, O (white color, Fig. 5e) corresponding to imide carbonyls and siloxane oxygen, and Si (yellow color, Fig. 5c) demonstrating that DDSQ cages and PDMS siloxane chains are well integrated throughout the polymer matrix without aggregation. TEM imaging (Fig. 5f) provides nanoscale structural insight into the hybrid PI film. Bright contrast domains (tens to hundreds of nanometers) are observed and correspond to the electron-dense DDSQ cages embedded within the darker organic polyimide matrix. These DDSQ-rich nanodomains are uniformly dispersed throughout the film without forming large clusters, confirming successful molecular-level integration of inorganic cages. The nanoscale dispersion observed by TEM is consistent with the homogeneous Si distribution shown in EDS mapping, demonstrating that DDSQ acts as well-distributed rigid nano-reinforcement within the flexible PDMS-containing imide framework. The combined spectroscopic, morphological, and elemental analyses confirm that PDMS and DDSQ segments are successfully co-incorporated and uniformly distributed within the hybrid polyimide film. The molecular-level compatibility between flexible siloxane chains and rigid silsesquioxane cages results in defect-free films with homogeneous elemental composition, which is critical for ensuring consistent mechanical and thermal performance.

Furthermore, the chemical structures and compositions of the synthesized PAA precursors were further analyzed by ^{1}H NMR spectroscopy, as shown in Figure S3. Characteristic signals corresponding to the PDMS segments and DDSQ units were clearly identified. The methyl protons of PDMS and DDSQ (–Si–CH$_3$) appeared at approximately 0.17 and 0.30 ppm, respectively. These well-resolved peaks enabled quantitative integration for compositional analysis. The PDMS/DDSQ ratios were estimated by comparing the integrated peak areas of the PDMS and DDSQ methyl protons The calculated compositions were found of DDSQ (21.5 %) for PDMS/DDSQ(8/2)-ND-ODA PAA, which is in good agreement with the targeted PDMS/DDSQ ratio of 80/20, confirming the successful incorporation of both segments into the polymer backbone and similar results are also observed in PPD-based system. These results provide direct evidence supporting the designed copolymer composition and validate the structure–property relationships discussed in this work.

Fig. 6 presents the FTIR comparison, SEM morphology, EDS elemental mapping, and TEM analysis for the PDMS/DDSQ-ND-PPD hybrid polyimide film. The FTIR spectra (Fig. 6a) show that the characteristic bands from PDMS-ND-PPD and DDSQ-ND-PPD are simultaneously retained in the hybrid precursor, confirming successful incorporation of both flexible PDMS and rigid DDSQ components. The preservation of Si–O–Si absorptions also indicates that the silsesquioxane cages remain structurally intact and the detail characterization of FTIR was also shown in Figure S2(f). SEM imaging (Fig. 6b) reveals a continuous film surface without large-scale phase separation, although slight surface roughness is observed compared with the ODA-based system, likely arising from the higher rigidity of the PPD segment. EDS elemental mapping demonstrates uniform spatial distribution of N, O, and Si (Fig. 6c-e) across the hybrid film, verifying homogeneous dispersion of the organic imide framework and inorganic siloxane/DDSQ components without large-scale aggregation. TEM (Fig. 6f) further confirms nanoscale dispersion of DDSQ cages within the polyimide matrix. Bright electron-dense domains corresponding to DDSQ are evenly distributed, while no large clustered regions are detected. Compared with the ODA analogue, the PPD-based hybrid exhibits a slightly denser and more compact nanoscale texture, consistent with the more rigid para-phenylene linkage. Overall, these results confirm that the PDMS/DDSQ-ND-ODA and PDMS/DDSQ-ND-PPD polyimide forms a well-integrated organic–inorganic hybrid film with homogeneous elemental distribution and uniformly dispersed DDSQ nanocages. Furthermore, the molecular weights and distributions of the synthesized poly(amic acid) (PAA) precursors were evaluated by gel permeation chromatography (GPC), and the results are summarized in Figure S4 and Table S1, which the molecular weights were estimated using polystyrene standards. All samples exhibited moderate molecular weights with relatively broad molecular weight distributions, which are characteristic of step-growth polymerization systems. The successful formation of polymeric PAA precursors was thus confirmed. In addition, the obtained molecular weights are sufficient to ensure good film-forming ability, consistent with the formation of uniform and mechanically stable films observed in this study. The differences in molecular weight among the samples may be attributed to the steric effects and reactivity differences of PDMS and DDSQ segments during polymerization.

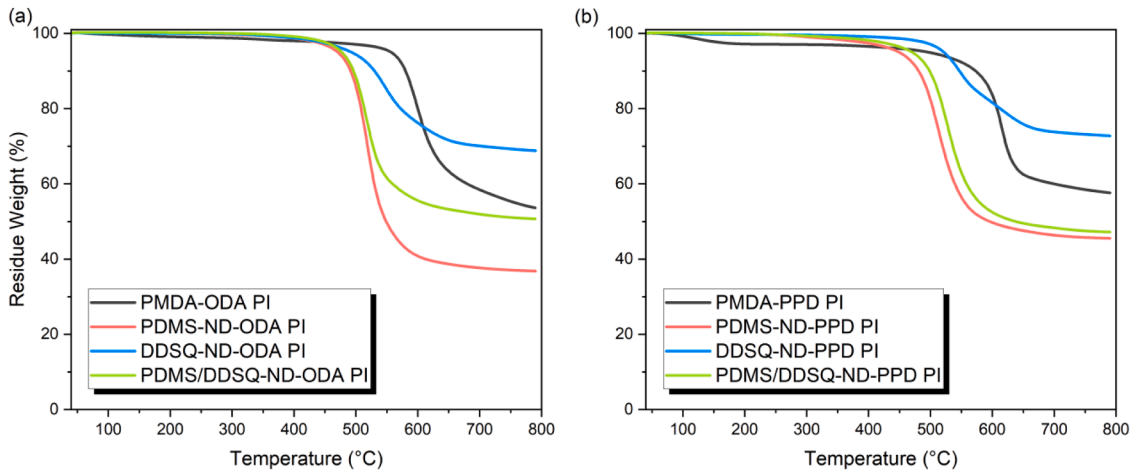

Fig. 7. TGA analyses of (a) PDMS/DDQ-ND-ODA PI and (a) PDMS/DDQ-ND-PPD PI system.

3.5. Thermal, mechanical, surface and dielectric properties of hybrid PDMS/DDSQ-Containing polyimides

Thermogravimetric analysis (TGA) was conducted to evaluate the thermal stability of the ODA- and PPD-based silicone polyimide systems (Fig. 7). For the ODA-based series (Fig. 7a), the fully aromatic ODA PI exhibits the highest onset stability (T_{d5} = 540 °C) because of its rigid imide backbone. Incorporation of flexible PDMS segments significantly reduces thermal resistance (T_{d5} = 471 °C) because of the thermally labile siloxane chains. In contrast, DDSQ-containing PI shows markedly enhanced stability (T_{d5} = 492 °C) and the highest char yield (68.8 wt %), reflecting the inorganic cage reinforcement. The hybrid PDMS/DDSQ-ND-ODA PI displays intermediate behavior, where DDSQ effectively compensates for PDMS-induced degradation, resulting in improved residual weight (50.7 wt %) compared with PDMS-only PI. A similar trend is observed in the PPD-based systems (Fig. 7b). The rigid PPD PI shows high thermal resistance (T_{d5} = 485 °C), while PDMS incorporation lowers stability (446 °C). DDSQ-based PI again exhibits superior thermal durability (T_{d5} = 520 °C) and the highest char yield (72.8 wt %). The hybrid PDMS/DDSQ-ND-PPD PI demonstrates balanced performance, maintaining elevated decomposition temperatures (T_{d5} = 469 °C) relative to PDMS-only PI, confirming that DDSQ cages serve as thermally stable inorganic nanofillers within the polyimide framework. Overall, these results demonstrate that DDSQ incorporation with 20 wt % significantly enhances thermal stability and char formation, while PDMS provides flexibility at the expense of thermal resistance. The hybrid PDMS/DDSQ systems successfully combine both effects, yielding polyimides with improved thermal robustness compared with PDMS-only analogues [20,29].

Figure S5 presents the tensile stress–strain behavior of pristine PMDA-ODA PI, PDMS and DDSQ-containing polyimides with different diamine structures. As shown in Figure S5(a), the pristine PMDA-ODA PI exhibits a steep initial slope and high tensile strength, reaching approximately 74.7 MPa with a strain at break of 6.7 %. The Young's modulus from the initial linear region is approximately 3.63 GPa, consistent with literature values for fully aromatic polyimides [44,45]. This behavior reflects the rigid backbone and strong intermolecular interactions of PMDA-ODA PI. In contrast to pristine PMDA-ODA PI, the

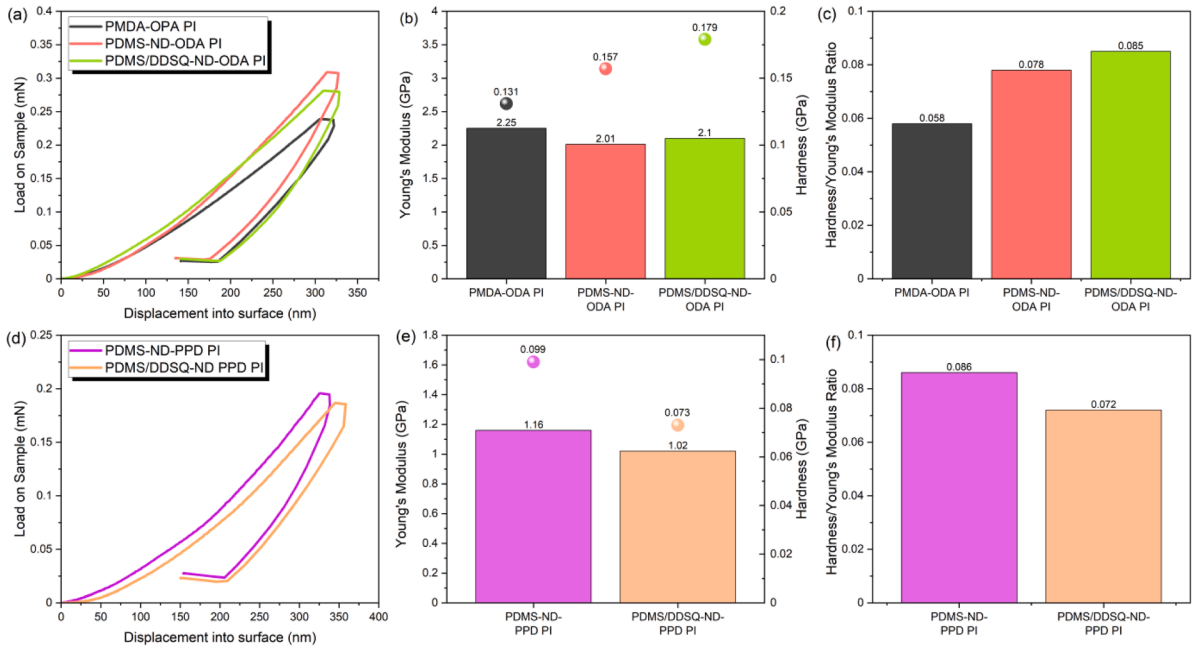

Fig. 8. Nanoindentation results of polyimide films. Load–displacement curves (left) and corresponding Young's modulus, hardness, and H/E ratio (right) for (a–c) ODA-based and (d–f) PPD-based systems with and without PDMS and DDSQ incorporation.

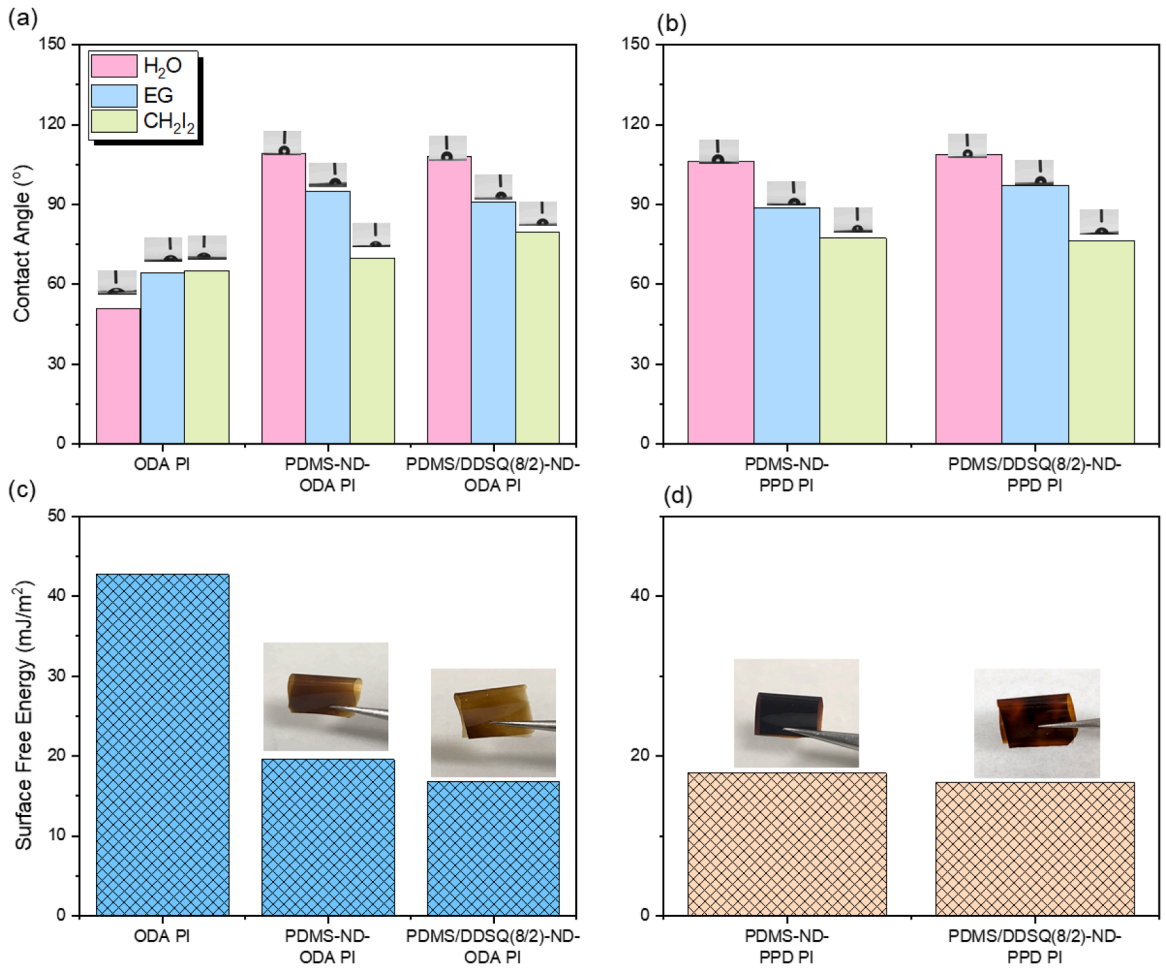

Fig. 9. Contact angle analyses and surface free energy of (a, c) PDMS/DDQ-ND-ODA PI system and (b, d) PDMS/DDQ-ND-PPD PI system.

PDMS-modified systems (Figures S5(c) and S5(d)) exhibit significantly reduced stiffness and tensile strength. For the ND-ODA-based systems (Figure S2(c)), both PDMS-ND-ODA PI and PDMS/DDSQ-ND-ODA PI show a gradual increase in stress followed by a plateau, with maximum stresses of approximately 29.1∼33.3 MPa. The incorporation of DDSQ results in a slightly higher modulus (from 1.13 GPa to 1.42 GPa) and strength (from 29.1 to 33.3 MPa), indicating a partial reinforcement effect due to its rigid inorganic structure. Similarly, for the ND-PPD-based systems (Figure S5(d)), both curves display a continuous increase in stress up to fracture, with lower ultimate stresses (∼20–22.6 MPa) and reduced elongation compared to the ND-ODA systems. The modulus in these systems is further decreased (0.98 GPa and 1.20 GPa), suggesting that the molecular structure of the diamine plays a critical role in determining mechanical performance. Overall, the incorporation of PDMS segments leads to a substantial decrease in modulus (from ∼3 GPa to ∼1 GPa), indicating reduced stiffness and enhanced mechanical compliance. Meanwhile, DDSQ incorporation slightly compensates for this softening effect by increasing rigidity. These results demonstrate that the mechanical properties can be effectively tuned through the combined design of flexible and rigid structural units.

Nanoindentation measurements were also performed to evaluate the surface mechanical properties of the polyimide films, and the results are summarized in Fig. 8(a) and (d). The pristine PMDA-ODA PI exhibits a Young's modulus of 2.25 GPa and hardness of 0.131 GPa (Fig. 8b), consistent with its rigid aromatic backbone. Upon incorporation of PDMS segments, a decrease in modulus is observed. For the PDMS-ND-ODA PI system, the modulus decreases to 2.01 GPa, while for the PDMS-ND-PPD system, a more pronounced reduction to 1.16 GPa is observed (Fig. 8e). This reduction reflects the increased chain flexibility and reduced intermolecular interactions introduced by the siloxane segments. The hardness shows a different trend, with PDMS-ND-ODA PI exhibiting an increased hardness (0.157 GPa) compared to pristine PMDA-ODA PI, suggesting localized resistance to deformation. In contrast, PDMS-ND-PPD PI shows a lower hardness (0.099 GPa), indicating a stronger softening effect depending on the diamine structure. The incorporation of DDSQ leads to a slight increase in modulus for the ND-ODA system (2.10 GPa) and modifies hardness values (0.179 GPa for ND-ODA and 0.073 GPa for ND-PPD systems), reflecting the competing effects between rigid inorganic cage structures and flexible polymer segments. Furthermore, the hardness-to-modulus ratio (H/E) increases upon PDMS and DDSQ incorporation (Figs. 8c and f), indicating enhanced resistance to plastic deformation and improved surface compliance. Overall, the nanoindentation results are in good agreement with the tensile measurements, confirming that the mechanical properties can be systematically tuned through molecular design.

The surface wettability of the prepared polyimide films was evaluated by static contact angle measurements using three probe liquids with different polarities, including deionized (DI) water, ethylene glycol, and diiodomethane (Fig. 9). The corresponding surface free energy values were calculated based on the Owens–Wendt method. For both ODA- and PPD-based systems, the pristine aromatic PIs exhibit moderate water contact angles (Fig. 9a), reflecting their relatively polar imide-rich surfaces [37]. Upon incorporation of PDMS segments, the water contact angle increases markedly, indicating enhanced hydrophobicity due to the low surface energy of siloxane chains and the outward migration of –Si(CH₃)₂– groups. The hybrid PDMS/DDSQ PIs show consistently

Table 1
The thermal, surface and dielectric properties of all PDMS and DDSQ-based hybrid PI materials.

Sample	T_{d5} (°C)	Char Yield (wt %)	Contact angle (°)			γ mJ/m^2	Dielectric Constant
			H_2O	EG	CH_2I_2		
PMDA-ODA PI	540	53.6	51.0	64.3	65.1	42.72	4.21
PDMS-ND-ODA PI	470	36.8	109.3	95.1	69.9	19.57	4.12
DDSQ-ND-ODA PI	492	68.8	Brittle (ND)				
PDMS/DDSQ-ODA PI	477	50.7	107.9	91.0	79.5	16.75	3.82
PMDA-PPD PI	484	57.6	Brittle (ND)				
PDMS-ND-PPD PI	446	45.5	106.2	88.8	77.4	17.87	3.39
DDSQ-ND-PPD PI	520	72.7	Brittle (ND)				
PDMS/DDSQ-PPD PI	469	47.2	108.8	97.1	76.3	16.66	3.24

higher contact angles for all probe liquids compared with the corresponding neat aromatic PIs, confirming that the silicone components dominate the surface characteristics. Among them, the PPD-based hybrids exhibit slightly larger water contact angles than the ODA analogues, attributable to the more rigid and less polar para-phenylene linkage that reduces surface polarity (Fig. 9b). Surface free energy analysis further supports these observations. The total surface energy decreases significantly after PDMS incorporation, mainly due to a reduction in the polar component. DDSQ-based PIs show higher dispersive contributions but lower polar fractions than pure aromatic PIs. The PDMS/DDSQ hybrid films present the lowest overall surface free energies, demonstrating synergistic effects between flexible PDMS chains and hydrophobic DDSQ cages. This reduction in surface energy correlates well with enhanced hydrophobicity and improved moisture resistance observed macroscopically (Fig. 9c and d). Since pure DDSQ-based PI system could not form the film to measure the related physical property; even though they possess the relative higher thermal properties. As a result, these results confirm that the introduction of silicone segments effectively tailors the PI surface from polar to hydrophobic by combination the balance between PDMS governing flexibility and DDSQ contributing inorganic, low-energy surface characteristics. Table 1 summarizes the thermal and surface properties of all PDMS and DDSQ-based hybrid PI materials. Furthermore, the surface morphology and phase behavior of the polyimide films were investigated by atomic force microscopy (AFM), as shown in Figure S6. The pristine ODA-based polyimide exhibits a relatively smooth surface with a low roughness value (Ra = 1.42 nm), indicating a homogeneous morphology. Upon incorporation of PDMS segments, the surface roughness increases significantly (Ra = 10.07 nm for PDMS-ND-ODA PI and 7.06 nm for PDMS-ND-PPD PI), which can be attributed to the introduction of flexible siloxane chains and their tendency to induce nanoscale heterogeneity. In contrast, the PDMS/DDSQ hybrid systems show reduced surface roughness (Ra = 1.52 nm for PDMS/DDSQ-ND-ODA PI and 4.17 nm for PDMS/DDSQ-ND-PPD PI) compared to the PDMS-only counterparts. This suggests that the incorporation of rigid DDSQ nanocages improves structural uniformity and suppresses excessive phase separation induced by PDMS segments. Overall, the AFM images reveal relatively homogeneous surface morphologies without obvious large-scale phase separation, indicating good compatibility between the organic polyimide matrix and the inorganic PDMS/DDSQ components. Notably, all samples exhibit surface roughness values below 100 nm, which is critical for the reliable determination of surface free energy in this study.

Fig. 10 compares the dielectric constants (k) of the aromatic polyimides and their PDMS/DDSQ-modified counterparts measured at 50 MHz. For the ODA-based system (Fig. 10a), the pristine aromatic PMDA-ODA PI exhibits a dielectric constant of 4.21. Incorporation of PDMS slightly lowers the k value to 4.12 due to the low polarity and flexible siloxane segments that reduce dipolar density. A further decrease is observed in the PDMS/DDSQ-ODA PI (k = 3.82), demonstrating that DDSQ cages effectively introduce nanoscale free volume and low-polarizable Si–O frameworks, leading to suppressed dielectric polarization. In the PPD-based series (Fig. 10b), the PDMS-ND-PPD PI shows a dielectric constant of 3.39, already lower than typical aromatic PIs because the rigid para-phenylene unit reduces chain polarizability. After incorporating DDSQ into the hybrid PDMS/DDSQ(8/2)-ND-PPD PI, the dielectric constant further decreases to 3.24. This significant reduction originates from the combined effects of the inorganic DDSQ nanocages and the low-polar PDMS segments, which collectively dilute the imide dipoles and increase internal free volume. Overall, the results confirm that DDSQ incorporation is highly effective in lowering dielectric constants in silicone polyimide systems, and the hybrid PDMS/DDSQ architecture provides the best dielectric performance among all samples.

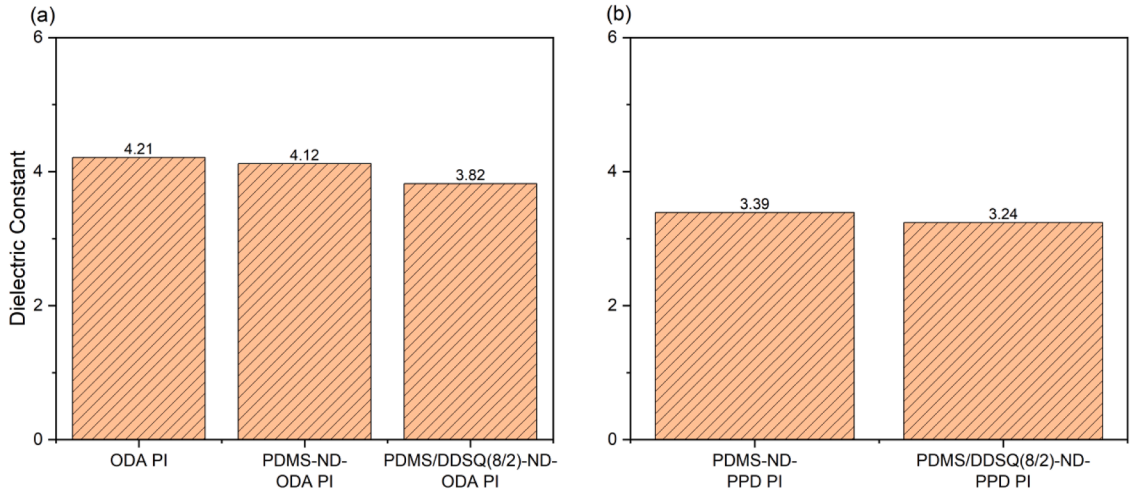

Fig. 10. Dielectric constants (k) of the aromatic PDMA-ODA polyimides and their (a) PDMS/DDSQ-ND ODA PI and (b) PDMS/DDSQ-ND PPD PI measured at 50 MHz.

4. Conclusions

Hybrid silicone–aromatic polyimides incorporating flexible PDMS segments and rigid DDSQ nanocages with diamine derivatives were successfully followed by PMDA-based step-growth polymerization and thermal imidization. The nadic-functionalization strategy enabled efficient introduction of reactive anhydride groups onto PDMS and DDSQ, which were subsequently converted into diamine-terminated silicone building blocks via nucleophilic ring opening with ODA and PPD. These well-defined intermediates provided a modular platform for preparing silicone-containing PAAs and their corresponding PI films. Spectroscopic analyses confirmed complete hydrosilylation, diamine incorporation, and successful imidization, while SEM, TEM, and elemental mapping revealed homogeneous film morphology and uniform nanoscale dispersion of DDSQ cages within the PDMS/PI matrix. The rigid DDSQ nanostructures significantly enhanced thermal stability and char yield (T_{d5} = 520 °C and char yield = 72.8 wt %), compensating for the lower thermal resistance introduced by flexible PDMS chains. The hybrid PDMS/DDSQ (80/20) systems achieved an optimal balance between flexibility and thermal robustness where the surface characterization demonstrated that silicone enrichment at the film interface reduced surface free energy (γ = 16.75 mJ/m^2) and increased hydrophobicity, thereby improving moisture resistance. Dielectric measurements further showed that the synergistic combination of low-polarizable PDMS segments and cage-type DDSQ units effectively suppressed dipolar polarization, leading to reduced dielectric constants compared with neat aromatic or PDMS-only polyimides (ε = 3.24). Overall, this work establishes a versatile synthetic route to integrate soft siloxane chains and rigid silsesquioxane nanocages into polyimide backbones, yielding hybrid films with tunable structure and enhanced thermal, surface, and dielectric performance suitable for advanced electronic and insulating applications.

CRediT authorship contribution statement

Hui-Wen Chen: Methodology, Investigation, Formal analysis, Data curation, Conceptualization. **Shiao-Wei Kuo:** Writing – review & editing, Writing – original draft, Supervision, Resources.

Declaration of competing interest

The authors declare that they have no known competing financial interests or personal relationships that could have appeared to influence the work reported in this paper.

Acknowledgments

This study was supported financially by the National Science and Technology Council, Taiwan, under contracts NSTC 114-2124-M-005-001. The authors thank the staff at National Sun Yat-sen University for their assistance with the TEM (ID: EM022600) experiments.

Supplementary materials

Supplementary material associated with this article can be found, in the online version, at doi:10.1016/j.jtice.2026.106802.

References

[1] Fu M-C, Higashihara T, Ueda M. Recent progress in thermally stable and photosensitive polymers. Polym J 2018;50:57–76. https://doi.org/10.1038/pj.2017.46.
[2] Dong X, Wan B, Zha J-W. Versatile landscape of low-k polyimide: theories, synthesis, synergistic properties, and industrial integration. Chem Rev 2024;124:7674–711. https://doi.org/10.1021/acs.chemrev.3c00802.
[3] Li H, Wei P, Wang Y, Zhu Q, Wang X, Gao W, Tao L, Ma K, Hu Z, Chen W. High-frequency 5G substrate: low dielectric biphenyl polyimide with low CTE and high thermal stability. Mater Today Adv 2024;23:100514. https://doi.org/10.1016/j.mtadv.2024.100514.
[4] Ke W-C, Lin J-W, Busireddy MR, Lee Y-H, Chen J-T, Hsu C-S. Enhancing the mechanical and dielectric properties of highly thermally stable polyimides via a crosslinkable bicyclo[2.2.2]oct-7-ene-2,3,5,6-tetracarboxylic dianhydride monomer. Polymer (Guildf) 2024;290:126495. https://doi.org/10.1016/j.polymer.2023.126495.
[5] Zhang Y, Zhang B, Wu Y, Wang T. Ultrahighly permeable carbon molecular sieving membranes enabled by blocking the precursor polyimide molecules with 6FAP moieties. J Taiwan Inst Chem Eng 2025;171:106906. https://doi.org/10.1016/j.jtice.2025.106096.
[6] Lu H, Shi J, Zhang X, Xu H, Wang X, Zhang T, Ming C, Zhao H, Li Y. Customizing adaptive thermoplastic polyimide interfaces in bismaleimide/boron nitride composites: a synergistic approach to achieving insulation and cyclic durability. Polym Compos 2026;47. https://doi.org/10.1002/pc.70367. in press.
[7] Wu Z, He J, Yang H, Yang S. Progress in aromatic polyimide films for electronic applications: preparation, structure and properties. Polymers (Basel) 2022;14:1269. https://doi.org/10.3390/polym14061269.
[8] Shen J, Jiang P, Wang Y, Zhang F, Li F, Tu G. Soluble sulfoxide biphenyl polyimide film with transmittance exceeding 90%. Polymer (Guildf) 2022;254:125050. https://doi.org/10.1016/j.polymer.2022.125050.
[9] Constantin C-P, Gradinaru LM, Plopa O, Rusu R-D. Surface modification of polyimide films towards very low contact angles. Polym Degrad Stab 2022;202:110036. https://doi.org/10.1016/j.polymdegradstab.2022.110036.
[10] Hsiao S-H, Ni Z-D. Synthesis and electrochromic properties of triphenylamine-based aromatic poly(amide-imide)s. Polymers (Basel) 2025;17:1152. https://doi.org/10.3390/polym17091152.
[11] Monleon QD, Thuillier QM, Soisson A, Chikh L, Banet P, Fichet O. Contribution of polymaleimide, pyromellitidiimide and polydimethylsiloxane units to the thermal stability of polyimide–silicone materials. Polym Degrad Stab 2023;214:110392. https://doi.org/10.1016/j.polymdegradstab.2023.110392.
[12] Huang H, Wu C, Wu SQ, Pan RQ, Yin LH, Jin XY, Pan YW, Wang HB, Yan XJ, Hong CQ, Han WB, Zhang XH. Super-flexible, thermostable and superhydrophobic polyimide/silicone interpenetrating aerogels for conformal thermal insulating and strain sensing applications. Chem Eng J 2022;441:136032. https://doi.org/10.1016/j.cej.2022.136032.
[13] Nie X, Qiao S, Xiao L, Wu J, Gao M, Li H, Zhang J, Tao D. Synergistic crosslinking and cage-structured POSS integrated in polyimides: toward ultra-low dielectric constant and high-resolution photolithography. Polym Chem 2025;16:2629–38. https://doi.org/10.1039/D5PY00236B.
[14] Liu LP, Lv FZ, Li PG, Ding L, Tong WS, Chu PK, Zhang YH. Preparation of ultra-low dielectric constant silica/polyimide nanofiber membranes by electrospinning. Compos Part A 2016;84:292–8. https://doi.org/10.1016/j.compositesa.2016.02.002.
[15] Parmeggiani M, Zaccagnini P, Stassi S, Fontana M, Bianco S, Nicosia C, Pirri CF, Lamberti A. PDMS/polyimide composite as an elastomeric substrate for multifunctional laser-induced graphene electrodes. ACS Appl Mater Interfaces 2019;11:33221–30. https://doi.org/10.1021/acsami.9b10408.
[16] Park J, Gaines KE, Jheng LC, Riffle JS, Mecham SJ, McGrath JE, Park HB, Paul DR, Freeman BD. Characterization and gas transport properties of UV-irradiated PDMS-containing polyimide copolymer membranes. Polymer (Guildf) 2020;210:122966. https://doi.org/10.1016/j.polymer.2020.122966.
[17] Xi K, Meng Z, Heng L, Ge RJ, He H, Yu XH, Jia XD. Polyimide–polydimethylsiloxane copolymers for low-dielectric constant and moisture-resistance applications. J Appl Polym Sci 2009;113:1633–41. https://doi.org/10.1002/app.30154.
[18] Mohamed MG, Ejaz M, Kuo S-W. Benzoxazine-linked polyhedral oligomeric silsesquioxane: 3D porous organic–inorganic polymer for improved CO_2 capture and supercapacitor performance. J Taiwan Inst Chem Eng 2025;171:106098. https://doi.org/10.1016/j.jtice.2025.106098.
[19] Kuo S-W, Chang F-C. POSS related polymer nanocomposites. Prog Polym Sci 2011;36:1649–96. https://doi.org/10.1016/j.progpolymsci.2011.05.002.
[20] Qiao G-Y, Wang X, Li J, Geng K, Jin E, Xu J-J, Yu J. Unlocking synthesis of polyhedral oligomeric silsesquioxane-based three-dimensional polycubane covalent organic frameworks. J Am Chem Soc 2024;146:3373–82. https://doi.org/10.1021/jacs.3c12650.
[21] Hsiao C-W, Mohamed MG, Kuo S-W. Structural design and functionalization of benzoxazine-modified octavinylsilsesquioxane hybrid porous polymer through Sonogashira coupling reaction. Mater Today Chem 2025;46:102795. https://doi.org/10.1016/j.mtchem.2025.102795.
[22] Ejaz M, Mohamed MG, Huang W-C, Kao Y-C, Chen W-C, Kuo S-W. Highly thermally stable polyhedral oligomeric silsesquioxane based on diacetal-functionalized polybenzoxazine nanocomposites. Eur Polym J 2025;223:113649. https://doi.org/10.1016/j.eurpolymj.2024.113649.
[23] Hsiao C-W, Elewa AM, Mohamed MG, Kuo S-W. Highly stable hybrid porous polymers containing POSS/dibenzo[g,p]chrysene and dibenzo[b,d]thiophene units for efficient Rhodamine B dye removal. Sep Purif Technol 2024;332:125771. https://doi.org/10.1016/j.seppur.2023.125771.
[24] Kao Y-C, Lin J-Y, Chen W-C, Mohamed MG, Huang C-F, Chen J-H, Kuo S-W. High-thermal-stable epoxy resin through blending nanoarchitectonics with double-decker-shaped polyhedral silsesquioxane-functionalized benzoxazine derivatives. Polymers (Basel) 2024;16:112. https://doi.org/10.3390/polym16010112.
[25] Mituła K, Januszewski R, Duszczak J, Rzonsowska M, Dudziec B. High thermally stable polysiloxanes cross-linked with di(alkenyl)functionalized DDSQs exhibiting swelling abilities. Eur Polym J 2022;171:111191. https://doi.org/10.1016/j.eurpolymj.2022.111191.

[26] Chen HW, Mohamed MG, Kao Y-C, Chen W-C, Chiou K, Kuo S-W. Overcoming synthetic challenges in developing high-performance polybenzoxazine from diamine-functionalized double-decker silsesquioxane cage. Eur Polym J 2025;232:113929. https://doi.org/10.1016/j.eurpolymj.2025.113929.
[27] Kim HJ, Mohamed MG, Yu HJ, Baek SH, Hossain I, Kuo S-W, Lee JS. Silica-based gas separation membranes: structure–performance relationships across the Si–O continuum from polysilsesquioxanes to amorphous SiO_2. J Membr Sci 2026;740:124907. https://doi.org/10.1016/j.memsci.2025.124907.
[28] Mohamed MG, Kuo S-W. Functional polyimide/polyhedral oligomeric silsesquioxane nanocomposites. Polymers (Basel) 2019;11:26. https://doi.org/10.3390/polym11010026.
[29] Pal S, Lu P-Y, Hung L-I, Lin C-H, Wang C-F. Preparation of fluorine-free superwetting metal–organic frameworks/polyhedral oligomeric silsesquioxane composites for oil absorption and exceedingly high flux emulsion separation. J Taiwan Inst Chem Eng 2025;172:106114. https://doi.org/10.1016/j.jtice.2025.106114.
[30] Wang H, Hang G, Hu J, Gao Y, Li L, Zheng S. Organic–inorganic polyimides with POSS cages in the main chains: impact of POSS R groups on morphologies and properties. ACS Appl Polym Mater 2023;5:4274–87. https://doi.org/10.1021/acsapm.3c00456.
[31] Yu W, Fu J, Dong X, Chen L, Shi L. A graphene hybrid material functionalized with POSS: synthesis and applications in low-dielectric epoxy composites. Compos Sci Technol 2014;92:112–9. https://doi.org/10.1016/j.compscitech.2013.12.016.
[32] Miao L, Zhan L, Liao S, Li Y, He T, Yin S, Wu L, Qiu H. Recent advances of polymer–POSS nanocomposites with low dielectric constant. Macromol Rapid Commun 2024;45:2300601. https://doi.org/10.1002/marc.202300601.
[33] Wu S, Hayakawa T, Kikuchi R, Grunzinger SJ, Kakimoto M. Synthesis and characterization of semiaromatic polyimides containing POSS in the main chain derived from double-decker-shaped silsesquioxane. Macromolecules 2007;40:5698–705. https://doi.org/10.1021/ma070547z.
[34] Wu S, Hayakawa T, Kakimoto M, Oikawa H. Synthesis and characterization of organosoluble aromatic polyimides containing POSS in the main chain derived from double-decker-shaped silsesquioxane. Macromolecules 2008;41:3481–7. https://doi.org/10.1021/ma7027227.
[35] Xiao Y, Lei X, Liu Y, Zhang Y, Ma X, Zhang Q. Double-decker-shaped phenyl-substituted silsesquioxane-based nanocomposite polyimide membranes with tunable gas permeability and good aging resistance. Sep Purif Technol 2023;315:123725. https://doi.org/10.1016/j.seppur.2023.123725.
[36] Prasad K, Rifai A, Recek N, Schuessler D, Levchenko I, Murdock A, Mozetič M, Fox K, Alexander K. Nanocarbon–polymer composites for next-generation breast implant materials. ACS Appl Mater Interfaces 2024;16:50251–66. https://doi.org/10.1021/acsami.4c08193.
[37] Li ZG. Self-healing system of superhydrophobic surfaces inspired from and beyond nature. Nanoscale 2023;15:1493–512. https://doi.org/10.1039/D2NR05952E.
[38] Chen CY, Chen WC, Mohamed MG, Kuo S-W. Highly thermally stable, reversible, and flexible main-chain-type benzoxazine hybrid incorporating both polydimethylsiloxane and double-decker-shaped polyhedral silsesquioxane units through Diels–Alder reaction. Macromol Rapid Commun 2023;44:2200910. https://doi.org/10.1002/marc.202200910.
[39] Chen CY, Mohamed MG, Chen WC, Kuo S-W. Construction of ultrastable porous carbon materials derived from organic/inorganic double-decker silsesquioxane hybrid as high-performance electrodes for supercapacitors. Mater Today Chem 2023;34:101773. https://doi.org/10.1016/j.mtchem.2023.101773.
[40] Chen ZY, Chen WC, Kuo S-W. Enhanced thermal and porous properties of double-decker-shaped silsesquioxane-bismaleimide nanocomposites for high-performance CO_2 storage and supercapacitors. Polym Chem 2024;15:553–64. https://doi.org/10.1039/D3PY01115A.
[41] Chen WC, Kuo S-W. Ortho-imide and allyl group effects on highly thermally stable polybenzoxazine/double-decker-shaped polyhedral silsesquioxane hybrids. Macromolecules 2018;51:9602–12. https://doi.org/10.1021/acs.macromol.8b02207.
[42] Huang YC, Chen WC, Kuo S-W. Mesoporous phenolic/POSS hybrids induced by microphase separation arising from competitive hydrogen bonding interactions. Macromolecules 2022;55:8918–30. https://doi.org/10.1021/acs.macromol.2c01585.
[43] Ban BS, Kim YB. Surface free energy and pretilt angle on rubbed polyimide surfaces. J Appl Polym Sci 1999;74:267–71. https://doi.org/10.1002/(SICI)1097-4628(19991010)74:2<267::AID-PP5>3.0.CO;2-#.
[44] Bvao F, Qi F, Lei H, Luo F, Cai Y, Dai X, Dong Z, Qiu X. Near-zero thermal expansion and high heat-resistance polyimide films based on a symmetric and rigid pyrazine structure. ACS Appl Polym Mater 2023;5:672–9. https://doi.org/10.1021/acsapm.2c01720.
[45] Li K, Zhang X, Qiao S, Wang X, Wang Z, Yan J, Zheng T. Fatigue resistant polyimide binders for high-performance SiOx/C anodes in lithium-ion batteries. ACS Appl Polym Matr 2025;7:278–86. https://doi.org/10.1021/acsapm.4c03043.